Energy & Environmental Science

Accepted Manuscript

ROYAL SOCIETY OF CHEMISTRY

www.rsc.org/ees

Journal Name

RSCPublishing

COMMUNICATION

Promoted C-C Bond Cleavage over Intermetallic $TaPt_3$ Catalyst toward Low-temperature Energy Extraction from Ethanol

Cite this: DOI: 10.1039/x0xx00000x

Received 00th January 2012,
Accepted 00th January 2012

DOI: 10.1039/x0xx00000x

www.rsc.org/

Rajesh Kodiyath,[a] Gubbala V. Ramesh,[a] Eva Koudelkova,[a] Toyokazu Tanabe,[a] Mikio Ito,[a] Maidhily Manikandan,[a] Shigenori Ueda,[b] Takeshi Fujita,[c] Naoto Umezawa,[a] Hidenori Noguchi,[a] Katsuhiko Ariga [d] and Hideki Abe*[a]*

Intermetallic $TaPt_3$ nanoparticles (NPs) are materialized for the first time and exhibit much higher catalytic performance than state-of-the-art Pt_3Sn NPs for the electrooxidation of ethanol. *In-situ* infrared-reflection-absorption spectroscopy (IRRAS) elucidates that the $TaPt_3$ NPs cleave the C-C bond in ethanol at lower potentials than Pt NPs, efficiently promoting the complete conversion of ethanol to CO_2. Single-cell tests demonstrate the feasibility of the $TaPt_3$ NPs as a practical energy-extraction catalyst for ethanol fuels, which realizes more than 2 times higher output currents than Pt-based cells at high discharge currents.

Small organic molecules (SOMs) including formic acid and alcohols are becoming crucial as environmentally-benign fuels for sustainable economy and society.[1] In particular, ethanol is of confocal interest because it contains the energetically dense C-C bond and can be produced via biochemical processes, possibly leading to carbon-neutral economy.[2,3] However, ethanol fuels are still precluded in widespread use except as an additive to petroleum for traditional combustion systems because of the lack in efficient catalysts which promote the complete oxidation of ethanol near room temperature, not being accompanied by heat loss.[3,4]

[a] *National Institute for Materials Science, 1-1 Namiki, Tsukuba, Ibaraki 305-0044, Japan*
E-mail. KODIYATH.Rajesh@nims.go.jp, ABE.Hideki@nims.go.jp
b Synchrotron X-ray Station at SPring-8, National Institute for Materials Science, 1-1-1 Kouto, Sayo, Hyogo, 679-5148, Japan
c WPI Advanced Institute for Materials Research, Tohoku University, Sendai 980-8577, Japan
d WPI International Center for Material Nanoarchitectonics, National Institute for Materials Science, 1-1 Namiki, Tsukuba, Ibaraki 305-0044, Japan

Pt catalysts can efficiently promote the complete electrooxidation of ethanol to carbon dioxide (CO_2) involving the C-C bond cleavage, but suffer from poor long-term activity due to severe catalytic poisoning by one of the reaction intermediates, carbon monoxide (CO-poisoning).[3b,5] Alloying Pt with late-*d*-metals or metalloids including Ru, Fe, Co, Ni, Cu or Sn improves both the CO-poisoning tolerance and catalytic activity toward C1-molecule fuels such as methanol and formic acid, but diminishes the catalytic activity toward the complete electrooxidation of ethanol.[3c,5b] In addition, the traditional binary-alloy catalysts lack long-term stability in repeated use because of surface segregation: the counter elements of Pt readily leach out of the alloy or migrate into the bulk during long-term operation at high overpotentials.[6]

It is acknowledged that the improved catalytic performance of the late-*d*-metal-Pt alloys for the C1 molecules is attributed to reaction-active OH admolecules, which are formed over the electropositive late-*d*-metal atoms in aqueous media and preferentially oxidize reaction intermediates on the neighboring Pt atoms (bi-functional mechanism).[7] Early-*d*-metals including Ta may be a rational alloy counterpart to Pt because Ta is much more electropositive and oxyphilic than the late-*d*-metals and can more favorably form the OH species to promote the desired, complete electrooxidation of ethanol.[8] Furthermore, the Ta-Pt alloys, when atomically ordered in an intermetallic phase of $TaPt_3$, can act as a more stable catalyst than conventional late-*d*-metal alloys because of its large enthalpy of formation: e.g., ΔH_f = -59.5 kJmol^{-1} of Ta for $TaPt_3$ compared with ΔH_f = -13.6 kJ mol^{-1} of Fe for Fe-Pt alloys.[9] However, synthesis of intermetallic $TaPt_3$ catalysts in the desired form of nanoparticles or porous materials has been a big challenge because of the extremely oxyphilic nature of Ta metal (Ta(0)).

In this communication, we report the first successful synthesis of intermetallic $TaPt_3$ in the form of nanoparticles ($TaPt_3$ NPs) and demonstrate their much enhanced activity

toward the electrooxidation of ethanol (EOR) in comparison to pure Pt NPs or state-of-the-art catalytic alloys, Pt_3Sn NPs. The $TaPt_3$ NPs also exhibit higher stability to 10000-times repeated EOR than Pt NPs or the alloy catalysts. Single-cell assembly comprising the $TaPt_3$ NPs as the anode catalyst has achieved higher power output than the reference cell comprising Pt catalysts. *In-situ* IRRAS has elucidated that the $TaPt_3$ NPs efficiently catalyze the C-C cleavage in ethanol at lower onset potentials than Pt NPs to promote the complete conversion of ethanol to CO_2.

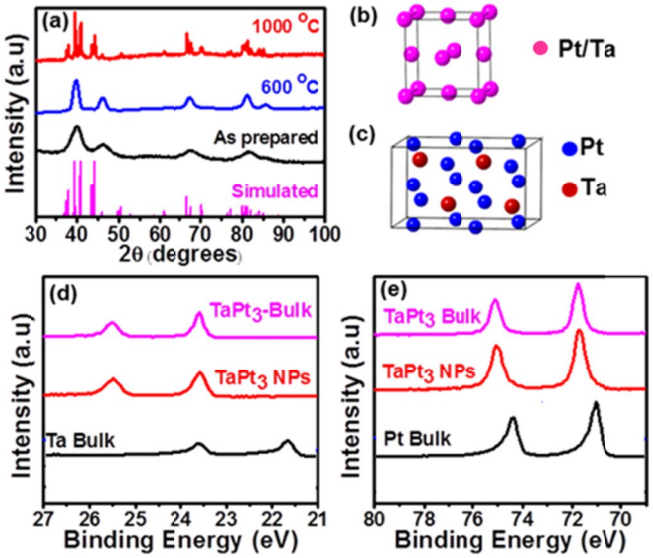

Figure 1. (a) *p*XRD profiles of Ta-Pt NPs (as-prepared and annealed at different temperatures). For comparison, the simulated *p*XRD pattern for intermetallic $TaPt_3$ is presented at the bottom. Structural models showing atomic arrangements in the Ta-Pt NPs (b) and $TaPt_3$ NPs (c). HX-PES spectra in the Ta 4*f*- (d) and Pt 4*f*- (e) regions for the $TaPt_3$ NPs. HX-PES spectra for bulk Pt, bulk Ta and bulk $TaPt_3$ are also shown as references.

The $TaPt_3$ NPs were synthesized by co-reduction of metal precursors in dry diglyme (See supporting information for the details). Figure 1a shows powder X-ray diffraction (*p*XRD) profiles of the as-prepared product and of the products annealed at different temperatures. Broad diffraction peaks are observed for the as-prepared product, indicating low crystallinity and/or small particle size. However, clear diffraction peaks appear when annealing the as-prepared product at high temperatures in vacuum. The product annealed at 600 °C exhibits five diffraction peaks at 39.7°, 46.2°, 67.3°, 81.2° and 85.6°, corresponding to the 111, 200, 220, 311 and 222 reflections of an fcc-type structure. The product annealed at 600 °C is consisted of alloy nanoparticles (Ta-Pt NPs) in which Ta and Pt are statistically distributed over the fcc lattice (Figure 1b). The calculated lattice parameter, a = 3.932 Å, is larger than that of pure Pt, a = 3.920 Å, showing the incorporation of larger Ta atoms in the Pt matrix to form the Ta-Pt phase. As the annealing temperature increases, additional peaks emerge from the intermetallic $TaPt_3$ phase (at 800 °C and 900 °C, Figure S1). The *p*XRD pattern for the product annealed at 1000 °C is fully assigned to intermetallic $TaPt_3$ ($NbPt_3$-type, space group $P21/m$, a = 4.869 Å, b = 5.537 Å, c = 9.269 Å, β = 100.62°, Figure 1b).[10]

Hard X-ray Photoemission spectra (HX-PES) of the $TaPt_3$ NPs show clear emission peaks from the metallic Ta(0) (Figure 1d). The binding energies of the Ta-core emissions from the $TaPt_3$ NPs are consistent with the values for bulk $TaPt_3$ (Figure 1d). Note that the Ta-core emissions from the $TaPt_3$ NPs are shifted to higher binding energies with respect to those from pure Ta metal, showing that the valence electrons of Ta atoms are used for the formation of Ta-Pt bonds to diminish the screening of the nucleus charge (Table S1). The formation of the Ta-Pt bonds also results in an increase in the binding energy of the Pt-core emissions from the $TaPt_3$ NPs, with respect to those of pure Pt (Figure 1e and Table S1).

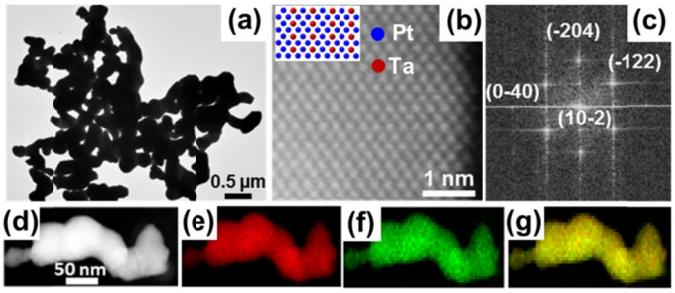

Figure 2. (a) TEM- and (b) STEM images of the $TaPt_3$ NPs. The inset shows a simulated atomic arrangement in the $TaPt_3$ NPs, viewed in the <201> direction. (c) FFT pattern obtained from Figure 2b. (d)-(g) EDS mapping of Pt (red), Ta (green) and the composite image for the $TaPt_3$ NPs.

Figure 2a shows that the prepared $TaPt_3$ NPs were agglomerated to form a network structure. The STEM image of a $TaPt_3$ NP and the corresponding FFT pattern indicate that the atoms in the $TaPt_3$ NPs are ordered in the monoclinic $NbPt_3$-type structure, as expected from *p*XRD (Figures 2b and 2c).[10] The EDS spectra have confirmed that the Ta- to Pt atomic ratio in the $TaPt_3$NPs is 1:3 (Figure S2). The compositional mapping over the $TaPt_3$ NPs is presented in Figures 2d-g. Importantly, the distributions of Pt (red) and Ta (green) are uniform over the $TaPt_3$ NPs, as is evident from the composite image (Figure 2g). The *p*XRD-, HX-PES- and TEM/STEM characterization have demonstrated that annealing of the as-prepared product at 1000 °C leads to the desired, single-phase $TaPt_3$ NPs.

The catalytic activity of the $TaPt_3$ NPs toward the ethanol-electrooxidation reaction (EOR) was tested in comparison with that of the Pt NPs and Pt-alloy NPs (Figure 3a and 3b). The electrooxidation currents were normalized with the electrochemical surface area (ECSA, SI).[11] The electrooxidation currents normalized to the Pt loading weight (mass activity) are shown in SI as Figure S3. The EOR peak-current density of the $TaPt_3$ NPs is 3 times higher than that of the Pt NPs (Figure 3a). The EOR onset potential of the $TaPt_3$ NPs, +0.27 V, is 0.17 V lower than that of the Pt NPs, +0.44 V. The $TaPt_3$NPs are superior to the state-of-the-art EOR

catalyst, carbon-supported Pt_3Sn NPs (Pt_3Sn/C), in terms of the higher current density and the lower onset potential (Figure 3b). One of the reasons for the enhanced activity of the $TaPt_3$ NPs is likely due to the ability of oxyphilic Ta reacting with water to form Ta-OH, which can further oxidize the reaction intermediates of alcohols chemisorbed onto the neighboring Pt atoms.[12]

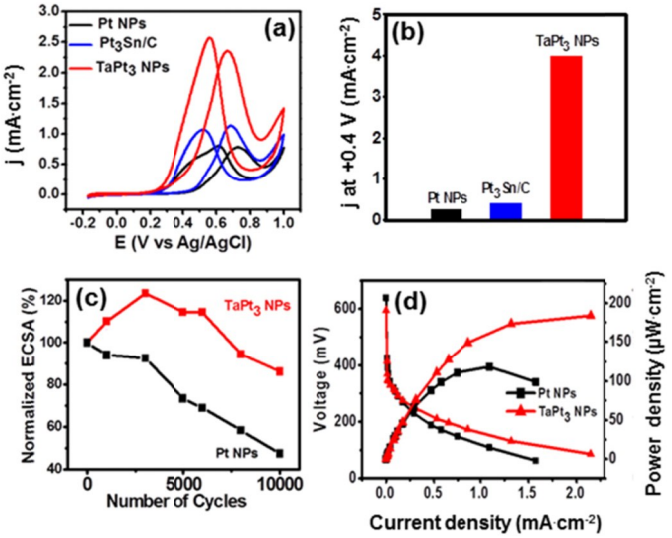

Figure 3. (a), (b) Cyclic voltammetry profiles for the $TaPt_3$ NPs and Pt NPs in 1.5 M ethanol solution. (c) Variation of ECSA of the $TaPt_3$ NPs and Pt NPs as a function of potential cycles. (d) I-V profiles and power density profiles of the $TaPt_3$ NPs and Pt NPs, obtained at room temperature in 1 M ethanol solution.

In order to investigate the long-term stability of the $TaPt_3$ NPs, we repeated potential cycles from -0.17 V to +1.0 V in 0.5 M H_2SO_4 solution. Figure 3c depicts the ECSA of the catalysts as functions of the number of cycles. The $TaPt_3$ NPs show good stability to repeated potential cycles: the $TaPt_3$ NPs retain 85 % of its initial ECSA even after 10000 cycles. The increase in ECSA of the $TaPt_3$ NPs, which is observed on the first few cycles, may be attributed to removal of contaminants from the catalyst surface, which is evident from the prominent hydrogen adsorption/desorption peaks (Figure S4).[13] EDS mapping after the stability test further confirmed that the $TaPt_3$ NPs retain their atomic arrangement and chemical composition intact even after the potential cycles (Figures S5 and S6). By clear contrast, the Pt NPs and Pt_3Sn/C retain only < 50 % of its initial ECSA after 10000 cycles, because of agglomeration and/or leaching of NPs (Figure S7).[14] These results of the stability test demonstrate that alloying of Pt with Ta significantly stabilizes the catalyst against harsh electrochemical conditions, possibly because the strong Ta-Pt bonds inhibit surface segregation and/or leaching during the catalysis.

We examined the feasibility of the $TaPt_3$ NPs as a practical energy-extraction catalyst for ethanol fuels by using a direct-ethanol-fuel-cell (DEFC) assembly (Figures S8 and S9). Figure 3d shows the *I-V* profiles and power-density profiles obtained for the different cell assemblies, each of them loaded the $TaPt_3$ NPs ($TaPt_3$-DEFC) or the Pt NPs (Pt-DEFC).[15] The $TaPt_3$-DEFC and the Pt-DEFC exhibited similar performance at low discharge currents. However, both the output potential and power output of the $TaPt_3$-DEFC became higher than those of the Pt-DEFC when the discharge current exceeded 0.15 mA·cm^{-2} (Figure S10). The power density of the $TaPt_3$-DEFC reached 215 μW at 1.6 mA·cm^{-2}, which was almost 2 times higher than that of the Pt-DEFC. This value was equal to 1/2 of the power density of a DEFC assembly comprising the state-of-the-art DEFC catalyst, Pt_3Sn/C, even though the particle size of the $TaPt_3$ NPs (>200 nm) was 100 times larger than that of the supported Pt_3Sn NPs (2~3 nm) (Figure S11 and Table S2). Note that the $TaPt_3$-DEFC, unlike Pt-DEFC, exhibited no degradation in power density at high current densities > 1 mA·cm^{-2}, showing inhibited polarization effects at the electrodes and improved tolerance to CO poisoning.[16] Indeed, CO-stripping tests (Figure S12) and density- functional-theory (DFT) calculations (Figure S13) have verified that the CO-chemisorption to the $TaPt_3$ surface is significantly weakened, resulting in the improved CO-poisoning tolerance which is competitive to that of the Pt_3Sn/C (Figure S12).

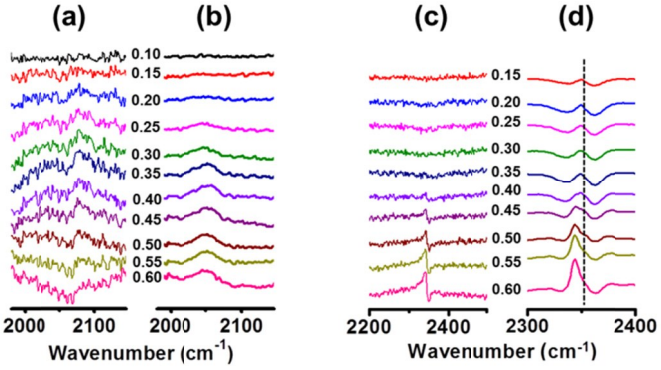

Figure 4. *In-situ* IRRAS spectra (from 1900 to 2500 cm^{-1}) over the $TaPt_3$ NPs (a) and Pt NPs. (b) *In-situ* IRRAS spectra (from 2200 to 2500 cm^{-1}) over the $TaPt_3$ NPs (c) and Pt NPs (d). The broken line in (d) situated at 2350 cm^{-1} corresponds to the peak position for atmospheric CO_2.

We further performed *in-situ* IRRAS measurements to elucidate the EOR kinetics over the $TaPt_3$ NPs (Figures 4a-4d). Figure 4a shows a series of IRRAS spectra for the $TaPt_3$ NPs in the CO-stretching region, acquired with increasing potentials (Figure S14). When the potential reaches +0.15 V, an anomaly becomes visible on the profile at 2070 cm^{-1}. This anomaly corresponds to the stretching mode of the CO molecules which are generated through cleavage of the C-C bond in ethanol.[17] The CO-stretching peak continuously grows with increase in potential up to +0.35 V, resulting in the enhanced EOR current in the potential range from +0.15 to +0.35 V (Figure 4a). The CO-stretching peak gradually

diminishes when the potential exceeds +0.40 V and finally becomes invisible at +0.60 V, as a result of the full conversion of CO admolecules to CO_2 (Figure S10). By contrast, CO evolves over the Pt NPs first at +0.25 V or higher potentials, which is consistent with literature (Figure 4b).[18] The $TaPt_3$ NPs are more active than Pt catalysts toward the C-C bond cleavage, in terms of the low onset potential for the CO generation.

The $TaPt_3$ NPs efficiently catalyze not only the C-C bond cleavage but also the complete conversion of ethanol to CO_2. As shown in Figure 4c, when the potential exceeds +0.35 V, the asymmetric stretching peak of CO_2 appears at 2342 cm^{-1} over the $TaPt_3$ NPs. The CO_2-stretching peak over the Pt NPs becomes first visible at +0.45 V, indicating that the Pt NPs are less active toward the complete ethanol/CO_2 conversion than the $TaPt_3$ NPs (Figure 4d, note that the IRRAS spectra contain background signals from atmospheric CO_2 at 2350 cm^{-1}).[19] Importantly, CO_2 starts to evolve over the $TaPt_3$ NPs at a similar potential to which the CO-stretching peak starts to decrease, +0.35 V (compare Figures 4a and 4c). In addition, the increase in the CO_2-streching peak at > +0.40 V (Figure 4c) is proportional to the decrease in the CO-stretching peak (Figure 4a). The enhanced ethanol/CO_2 conversion over the $TaPt_3$ NPs is primarily attributed to the electrooxidation of the CO admolecules.

In conclusion, we have successfully developed a high-performance alcohol-electrooxidation catalyst, $TaPt_3$ NPs. The $TaPt_3$ NPs are superior to state-of-the-art binary alloy catalysts in terms of the stability and catalytic activity toward the electrooxidation of ethanol. *In-situ* IRRAS measurements have elucidated that the $TaPt_3$ NPs efficiently promote both the C-C bond cleavage in ethanol and the complete conversion of ethanol to CO_2. Moreover, single-cell tests have demonstrated that the $TaPt_3$ NPs act as a highly feasible catalyst for the desirable low-temperature energy extraction from ethanol fuels. The large particle size of the current $TaPt_3$ NPs limits the figure of merit of $TaPt_3$ NPs-based catalysts. However, the particle size of catalysts can be significantly reduced by dispersing the NPs over appropriate electro-conductive supports, such as carbon nanoparticles or graphenes (Figure S15).[20] The molecular kinetics of the promoted C-C bond cleavage and CO_2 evolution over the $TaPt_3$ surface is currently being investigated. The developed, high-performance $TaPt_3$ NPs electrocatalyst may prompt the low-temperature energy management based on ethanol fuels, meeting the energy/environmental challenges presently we face.

Acknowledgement

This work was preliminarily supported by the JST PRESTO program, the Ministry of Education, Culture, Sports, Science and Technology (MEXT). The HX-PES measurements were performed under the approval of the NIMS Synchrotron X-ray Station (Proposal No. 2012B4609, 2013A4600, 2014A4603). The authors are grateful to HiSOR, Hiroshima University, and JAEA/SPring-8 for the development of HX-PES at BL15XU of Spring-8. We thank Dr. Oruganti Anjaneyulu for his help in obtaining Fuel Cell Data.

Electronic Supplementary Information (ESI) available:
Synthetic procedures, *p*XRD profiles, HX-PES spectra, EDS spectra, details of electrochemical measurements, DFT simulations are provided in the SI. This material is available free of charge via the Internet at http://.

Notes and references

1. a) G. Ertl, H. Knözinger, and J. Weitkamp, *Handbook of Heterogeneous Catalysis*, VCH, Weinheim, 1997. b) M. K. Debe, *Nature*, 2012, **486**, 43. c) H. Liu, C. Song, L. Zhang, J. Zhang, H. Wang, and D. P Wilkinson, *J. Power Sources*, 2006, **155**, 95. d) C. Lamy, A. Lima, V. LeRhun, F. Delime, C. Coutance, and J-M. Leger, *J. Power Sources*, 2002, **105**, 283. e) C. Bianchini and P. K. Shen, *Chem. Rev*., 2009, **109**. 4183. f) N. M. Aslam, M. S. Masdar, S. K. Kamarudin, and W. R. W. Daud, *APCBEE Procedia***,** 2012, **3**, 33. g). X. Yu, and P. G. Pickup, *J. Power Sources*, 2008, **182**, 124.
2. a) M. Z. F. Kamarudin, S. K. Kamarudin, M. S. Masdar, and W. R. W. Daud, *Int. J. Hydrogen Energy*, 2013, **38**, 9438. b) A. Brouzgou, A. Podias, and P. Tsiakaras, *J. Appl. Electrochem*., 2013, **43**, 119.
3. a) S. Song and P. Tsiakaras, *Appl. Catal. B*: *Environ.,* 2006, **63**, 187. b) C. Lamy, S. Rousseau, E. M. Belgsir, C. Coutanceau, and J. M. Leger, *Electrochim. Acta*, 2004, **49**, 3901. c) Z. F. Xu and Y. Wang, *J. Phys. Chem. C,* 2011, **115**, 20565.
4. a) R. Kavanagh, X. M. Cao, W. F. Lin, C. Hardacre, and P. Hu, *Angew. Chem. Int. Ed*., 2012, **51**, 1572. b) J. C. M. Silva, L. S. Parreira, R. F. B. De Souza, M. L. Calegaro, E. V. Spinace, A. O. Neto, and M. C. Santos, *Appl. Catal. B*, 2011, **110**, 141.
5. a) F. H. B. Lima and E. R. Gonzalez, *Electrochim. Acta*, 2008, **53**, 2963. b) Q. Wang, G. Q. Sun, L. H. Jiang, Q. Xin, S. G. Sun, Y. X. Jiang, S. P. Chen, Z. Jusys, and R. J. Behm, *Phys. Chem. Chem. Phys*., 2007, **9**, 2686.
6. a) S. Alayoglu, P. Zavalij, B. Eichhorn, Q. Wang, A. I. Frenkel, and P. Chupas, *ACS Nano*, 2009, **3**, 3127. b) D. Xu, Z. Liu, H. Yang, Q. Liu, J. Zhang, J. Fang, S. Zou, and K. Sun, *Angew. Chem., Int. Ed.,* 2009, **48**, 4217. c) X. Ji, K. T. Lee, R. Holden, L. Zhang, J. Zhang, G. A. Botton, M. Couillard, and L. F. Nazar, *Nat. Chem*., 2010, **2**, 286.
7. a) T. Iwasita and E. Pastor, *Electrochim. Acta,* 1994, **39**, 531. b) F. Vigier, C. Coutanceau, F. Hahn, E. M. Belgsir, and C. Lamy, *J. Electroanal. Chem*., 2004, **563**, 81.
8. a) Landolt-Börnstein data base; Springer, Berlin, 2002. b) B. deB. Darwent, NSRDS-NBS *31*, 1970.
9. A. R. Miedema, R. Boom, and F. R. De Boer, *J. Less-Common Met*., 1975, **41**, 283.
10. B. C. Giessen, R. H. Kane, N. J. Grant, *Trans. Metall. Soc. AIME*, 1965, **233**, 855.
11. Y. J. Gu and W. T. Wong, *Langmuir*, 2006, **22**, 11447.
12. M. Krausa and W. Vielstich, *J. Electroanal. Chem*., 1994, **379**, 307.
13. D. Wang, H. L. Xin, R. Hovden, H. Wang, Y. Yu, D. A. Muller, F. J. Disalvo, and H. D. Abruna, *Nat. Mater*., 2013, **12**, 81.
14. a) Z. Chen, M. Waje, W. Li, and Y. Yan, *Angew. Chem., Int. Ed*., 2007, **46**, 4060. b) B. Y. Xia, H. B. Wu, Y. Yan, and X. W. Lou, *J. Am. Chem. Soc.,* 2013, **135**, 9480.
15. J. P. Pereira, D. S. Falcao, V. B. Oliveira, and A. M. F. R. Pinto, *J. Power Sources*, 2014, **256**, 14.
16. J. Shim, J. Lee, Y. Ye, J. Hwang, S. K. Kim, T. H. Lim, U. Wiesner, and J. Lee, *ACS Nano*, 2012, **6**, 6870.
17. a) Z. Peng, C. Kisielowski, and A. T. Bell, *Chem. Commun*., 2010, **48**, 1854. b) C. Zhang, S. Y. Hwang, A. Trout, and Z. Peng, *J. Am. Chem. Soc.,* 2014, **136**, 7805.
18. J. M. Leger, S. Rousseau, C. Coutanceau, F. Hahn, and C. Lamy, *Electrochim. Acta*, 2005, **50**, 5118.
19. a) T. Herranz, M. Ibanez, J. L. Gomez de la Fuente, F. J. Perez-Alonso, M. A. Pena, A. Cabot, and S. Rojas, C*hem. Electrochem*., 2014, **1**, 885. b) N. Erini, R. Loukrakpam, V. Petkov, E. A. Baranova, R. Yang, D. Teschner, Y. Huang, S. R. Brankovic, and P. Strasser, *ACS Catal*. 2014, **4**, 1859. c) A. Kowal, M. Li, M. Shao, K. Sasaki, M. B. Vukmirovic, J. Zhang, N. S. Marinkovic, P. Liu, A. I. Frenkel, and R. R. Adzic, *Nat. Mater*. 2009, **8**, 325. d).W. P. Zhou, M. Li, C. Koenigsmann, C. Ma, S. S. Wong, and R. R. Adzic, *Electrochim. Acta*, 2011, **56**, 9824.
20. a) S. Guo and S. Sun, *J. Am. Chem. Soc*., 2012, **134**, 2492. b) H. Qiu, X. Dong, B. Sana, T. Peng, D. Paramelle, P. Chen, and S. Lim, *ACS Appl. Mater. Interfaces,* 2013, **5**, 782.

Journal Name

COMMUNICATION

TOC

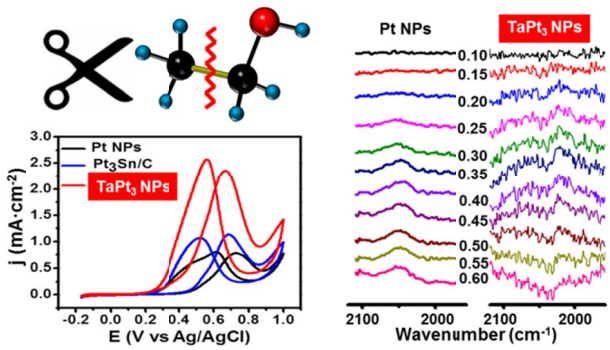

Intermetallic $TaPt_3$ nanoparticles (NPs) efficiently promote C-C bond cleavage in ethanol and exhibit much higher catalytic performance than any of the traditional binary-alloy catalysts for the ethanol electrooxidation.

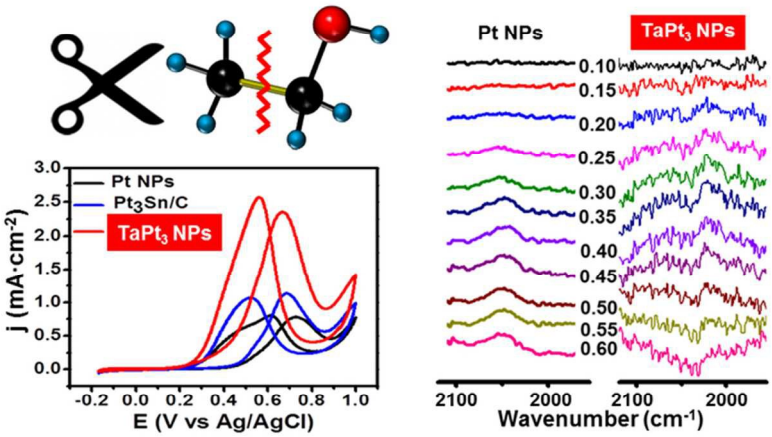

Intermetallic $TaPt_3$ nanoparticles (NPs) efficiently promote C-C bond cleavage in ethanol and exhibit much higher catalytic performance than any of the traditional binary-alloy catalysts for the ethanol electrooxidation.
62x91mm (300 x 300 DPI)